

NUMERICAL MODELLING OF HUMAN BODY FOR BLUETOOTH BODY-WORN APPLICATIONS

Masood Ur-Rehman^{1, 2, *}, Qammer Hussain Abbasi^{3, 4}, Xiaodong Chen², and Zhinong Ying⁵

¹Centre for Wireless Research, University of Bedfordshire, Park Square, Luton LU1 3JU, UK

²School of Electronic Engineering and Computer Science, Queen Mary University of London, Mile End Road, London E1 4NS, UK

³Texas A & M University, Qatar Campus, Qatar

⁴University of Engineering and Technology, Lahore, Pakistan

⁵Sony Ericsson Mobile Communications AB, Lund, Sweden

Abstract—The human body has got a pivotal role in portable devices operating in Body-centric Wireless Networks (BCWNs). Electromagnetic interaction between lossy human body tissues and wearable antennas degrades the system performance. Efficient deployment of such systems necessitates thorough understanding of these effects. Numerical analysis is a powerful tool that provides useful information of such scenarios fairly quicker than the actual measurements giving the user full control of the design environment. This paper investigates usefulness of numerical analysis based on the comparison of three different homogeneous models of the human body. Effectiveness of a numerical model is evaluated in terms of its resolution, computational efficiency, time consumption and accuracy of the results in software followed by experimental verifications.

1. INTRODUCTION

Wireless communication technology has seen great advancements in recent years. This along with continuous demand of convergence of multiple technologies with ease of portability, mobility, flexibility, unobtrusiveness, low cost, low weight and miniaturisation has lead to

Received 4 August 2013, Accepted 24 November 2013, Scheduled 6 December 2013

* Corresponding author: Masood Ur-Rehman (masood.urrehman@beds.ac.uk).

a new wave of wearable devices. Increasing presence of such devices in our daily life has resulted in the development of Body-centric Wireless Networks (BCWNs). These networks consist of multiple wireless sensors placed on or near the human body. Applications of the BCWNs span healthcare, navigation and positioning, entertainment, security and surveillance, space exploration and military [1, 2]. The human body is an inherent part of the BCWN applications. As these applications use the wireless medium of propagation, they are vulnerable to electromagnetic distortions caused by the varying electric properties of the lossy human body tissues. It is now a well established fact that the performance of the BCWN antennas operating in close proximity of the human body is degraded due to distortion in radiation pattern, reduction in radiation efficiency and de-tuning of input impedance [1, 3–8].

Efficient deployment of the BCWN systems makes it indispensable to evaluate the interaction of the human body and body-worn antennas. Measurement campaigns with human subjects have disadvantages of uncontrollable movements, longer experimental durations, lack of repeatability and pose health and safety hazards [5, 9]. Human body modelling is an alternative approach that can be accomplished either experimentally or numerically. Experimental modelling involves use of physical phantoms made from solid, liquid or gel materials while numerical modelling is based on body phantoms embedded in electromagnetic codes. Use of physical phantoms is limited due to greater cost and lower flexibility in terms of body shape and posture [10]. Modern software solutions of the Maxwell's equations like finite difference time domain (FDTD) and method of moment (MoM) with efficient 3-D modelling of large practical scenarios not only remove the drawbacks of measurements but also provide overview of the expected on-body performance of the antennas and a means to validate the results through comparison of simulation and measurement.

Size of the problem (i.e., voxel size) and definition of the input play an important role to govern the accuracy of the results obtained using any numerical method. It is a process where all inputs like geometry and electrical properties of the model are adjusted to get an output with acceptable precision. A good solution provides a balance between the precision of the outputs, required computational resources and simulation times. Therefore, it needs characterisation of different types of the human body models. A wide variety of numerical human body phantoms have been used in the literature ranging from simple canonical models to complex voxel models. Simple models include homogeneous or layered flat models [11] used to evaluate

electromagnetic effects where energy is radiated from simple sources like a plane wave or small dipole antenna, spherical models used to evaluate electromagnetic effects inside the human head [12,13], and cylindrical models [8,14] used to evaluate the electromagnetic effects of the whole-body presence. Advancement in medical imaging techniques like magnetic resonance imaging (MRI) along with greatly enhanced computing power and software approaches has made it possible to develop detailed realistic homogeneous and inhomogeneous head and whole-body models composed of many voxels [1,4–7,15]. Human-head models are usually used for the characterisation of mobile terminal antennas when placed near to the head in talking position [5,16]. Whole-body voxel models with a spatial resolution as high as 1 mm^3 have been developed to represent humans of different physique and classify more than 30 different types of human body tissues [10,17]. CST Microwave Studio[®] has collaborated with Visible Human Project[®] and enables the import of Voxel Man which is based on a layered model obtained using a dissected male corpse [20]. Different on-body scenarios with varying body postures and on-body antenna positions can be easily simulated importing these models in electromagnetic numerical tools.

The low resolution models consisting of human body parts like head, hand or arm cannot provide full account of the complete human body effects while high resolution realistic body models require huge computational resources and are very time consuming. For the efficient work flow, a compromise between resources, time and accuracy of results plays a crucial role. This paper presents characterisation of three numerical models for human body having different resolutions based on comparative analysis to study their efficiency and find a suitable modelling approach for body-mounted Bluetooth applications. A planar inverted F antenna (PIFA) on the mobile phone handset and a meander line monopole antenna on the headset have been used in this study. A thorough numerical modelling, supported by the measurements, has been carried out to highlight the importance of numerical modelling and its benefits in terms of computational efficiency, time consumption and accuracy of the results.

2. ANTENNAS FOR ON-BODY COMMUNICATION

Two commercially available antennas operating at 2440 MHz are used in this study. The antennas were designed numerically and tested experimentally by the authors and results have been reported in a previous study [18]. As a continuation of the previous work, this study employs the same two antennas.

The headset antenna is a meander line monopole antenna fed using a discrete port with $50\ \Omega$ impedance to represent the commonly used $50\ \Omega$ coaxial port. It has a -10 dB bandwidth of 592 MHz, ranging from 2142 MHz to 2734 MHz. The simulated peak gain is noted to be 2.7 dBi. A Planar Inverted F Antenna (PIFA) is used as the mobile handset antenna. The PIFA is mounted on a ground plane of $100\ \text{mm} \times 40\ \text{mm}$ and fed by a $50\ \Omega$ coaxial port. It has -10 dB bandwidth of 206 MHz in the required frequencies and peak gain of 4.1 dBi.

3. NUMERICAL MODELLING OF HUMAN BODY

The choice of the right model for the study of body effects is very critical as computational efficiency decreases with increase of model resolution and its size. In this work, the on-body communication link has been studied for three different human body models to assess the computational difficulties and impact on the accuracy of the results. Measurement results are used as a reference to benchmark the working of the three models and recommend a viable solution in terms of accuracy and computational efficiency.

CST Microwave Studio[®] has been used to develop the three numerical models of the human body. Due to the complexity of the human body composition, these models are designed employing single layer homogeneous structure by averaging the tissue properties estimating weight of the main tissue contents. They are approximated to include 10% skin, 30% fat, 40% muscle and 20% bone (average of Bone Concancellous, Bone Cortical and Bone Marrow), which results in an weighted averaged relative permittivity of 28.81 and conductivity of 1.02 S/m at 2440 MHz. The values for the four types of tissues at 2440 MHz used in this study are summarised in Table 1.

Table 1. Electric properties of specific human tissues at 2440 MHz used within the constructed homogeneous body models [19].

Tissue	Electric Properties	
	Dielectric Constant (ϵ_r)	Tissue Conductivity (σ) (S/m)
Average Bone	11.74	0.43
Fat	5.28	0.11
Muscle	52.74	1.73
Skin	38.01	1.46

The meshing scheme is made adaptive where finer cell sizes have been used around the vital parts of the body. This method reduces the required number of cell volumes (voxels) in the computational domain significantly, hence the computation and time requirements. The Perfectly Matched Layer (PML) absorbing boundary conditions are implemented [20] having a maximum mesh cell size of 10 mm near the boundaries of the computational domain and a minimum mesh cell size of 0.08 mm at the edges of the solids in the computational domain.

The high level discretisation of the whole-body model represents an average built human with a height of 1755 mm, as shown in Figure 1(a). This very realistic model based on MRI scans was developed by the Dstl, UK [17]. The authors made necessary adjustments to make it compatible with CST Microwave Studio®. This model is rigid and replicates a standing human subject.

To obtain a medium resolution model, the high-resolution human body model is modified keeping the head as a high-resolution object while simplifying remaining organs, as illustrated in Figure 1(b). This

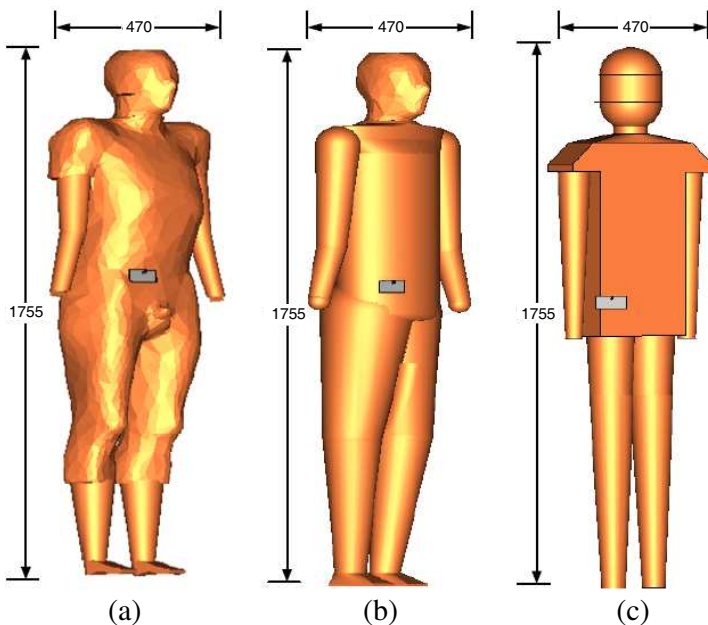


Figure 1. Structure of realistic high-resolution, simplified medium-resolution and basic low-resolution numerical models of the human body with on-body positioned headset and handset antennas (all lengths are in mm). (a) High-resolution model. (b) Medium-resolution model. (c) Low-resolution model.

medium-resolution model represents a nearly realistic shape of an average built human with a height of 1755 mm and thickness of 220 mm. This model has benefits of reduced complexity and flexibility in terms of re-positioning body parts (e.g., sitting, standing, talking and holding phone positions).

Finally, a low-resolution simpler homogeneous model based on canonical geometries is developed, as depicted in Figure 1(c). The complete height of this low-resolution body model is 1755 mm. The thickness of the torso for this low-resolution model is 120 mm while radius of the head is 86 mm.

4. PERFORMANCE EVALUATION OF HUMAN BODY MODELS

The performance of the three numerical models have been studied for on-body Bluetooth transmission using computer simulations in terms of transmission coefficient, radiation patterns, electric field distribution and specific absorption rate (SAR).

4.1. On-body Transmission

Impact of different resolutions and shapes of the numerical models of the human body on the Bluetooth link between the body-worn handset and headset antennas is studied. The Bluetooth link is characterised in terms of average path gain (S_{21}). The placement of the headset and handset antennas are kept similar for the three models to achieve a fair comparison. The separation between the body surface and the two antennas is 10 mm in order to incorporate the clearance for the cover assembly. The headset antenna is placed near the head at approximate location of the ear. Its ground plane is longitudinal in y -axis. The handset antenna is placed on right side of the body model at waist realising a typical body-worn position. The ground plane of the handset antenna is longitudinal in x -axis with the PIFA at the top of the ground plane as depicted in Figure 2(a).

The numerical modelling of the human body is validated by confirming the simulated results through measurements of on-body Bluetooth communication link. An Agilent HP8720ES Vector Network Analyser is used for the measurements. The prototypes of the two Bluetooth antennas used in the measurements are shown in Figure 2(b). The measurement set-up in an anechoic chamber is illustrated in Figure 2(c). First, the Bluetooth link is studied in the absence of the human body for the sake of bench-marking. In this scenario, the handset PIFA antenna and the headset meander line

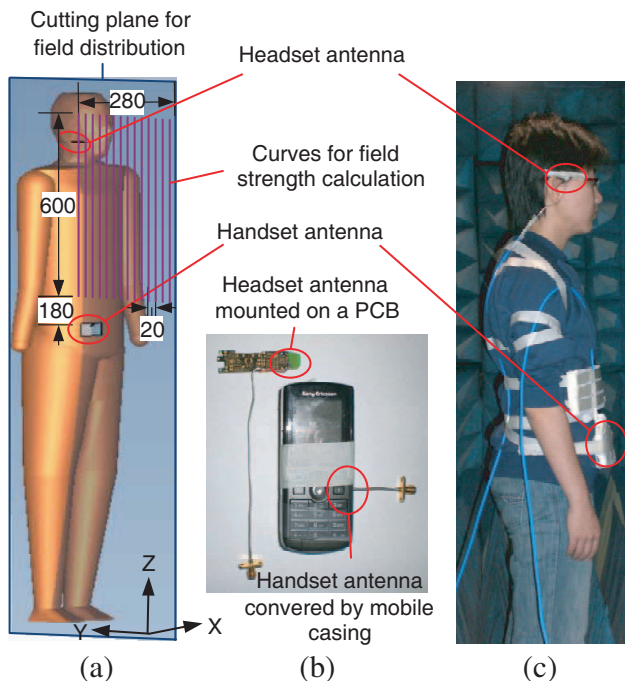


Figure 2. Simulation set-up (showing on-body test configurations with headset and handset antenna positions, location of cross-section plane and definition of curves for the observation of electric field distribution), antenna prototypes and measurement set-up in anechoic chamber (all lengths are in mm). (a) Simulation set-up. (b) Antenna prototypes. (c) Measurement set-up.

monopole antenna are placed exactly at the same locations where they would be in the presence of the human body. Therefore, the test set-up is essentially the same as described in Figure 2(a), but without the presence of the human body model. To locate these exact positions, a cube of polystyrene replicating the on-body gap between the two antennas was used in measurements. The two antennas are fed by low-loss coaxial cables of 5 m length. It is observed that the direct link between the handset and the headset antenna is -36.8 dB in simulation and -36.5 dB in measurement at 2440 MHz, as illustrated in Figure 3.

The Bluetooth link is then investigated for the on-body transmission with body-worn handset and headset antennas. Simulated results for the three body models are compared and validated through measurements. In the experiment, the headset and handset antennas have been worn by a volunteer and arranged in the same configura-

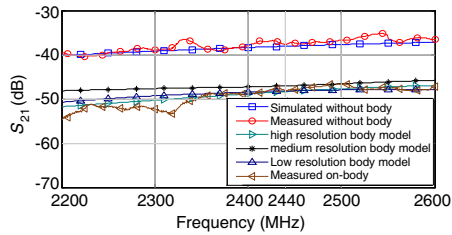


Figure 3. Comparison of simulated and measured average path gains for Bluetooth headset and handset antennas at 2440 MHz.

tions as were modelled as shown in Figure 2. The coupling between the two low-loss feed cables is measured separately and a loss variation of 0.5 dB (maximum) is found on-body. The measured path gain between the body-worn handset and the headset is found to be -48.1 dB at 2440 MHz. This value is noted to be -48.3 dB, -47.7 dB, and -49.5 dB in simulation for the high, medium and low resolution models respectively, as indicated in Figure 3. In the presence of the human body, the path gain value sees a substantial drop of 11.3 dB in measurement while 11.5 dB, 10.9 dB and 12.7 dB in simulation using high, medium and low resolution body models respectively. This drop is not surprising as the body blocks the line-of-sight between the headset and handset antennas.

It is evident from the close agreement of the measured and simulated path gain values that the three models are a good approximation of the real human subject. Moreover, from the good agreement of the measured path gain and simulated values for high and low resolution models, it can be deduced that for this communication link, a very simple homogeneous body model that utilises less computing resources and offers higher time efficiency can provide results as accurate as obtained using very detailed body representations.

Overall, the simulated path gains have shown a good agreement to the measured value. Few discrepancies are associated to small differences between the computer model and the experiment, such as the shape of the body, tissue properties, presence of clothes and feeding cables. This close agreement between the two values not only validates the numerical modelling approach and designed computer models but also serves as a benchmark for further investigation.

4.2. Effects on Antenna Radiation Pattern

The three designed models are used to investigate the impact of body shape and resolution on the radiation characteristics of the

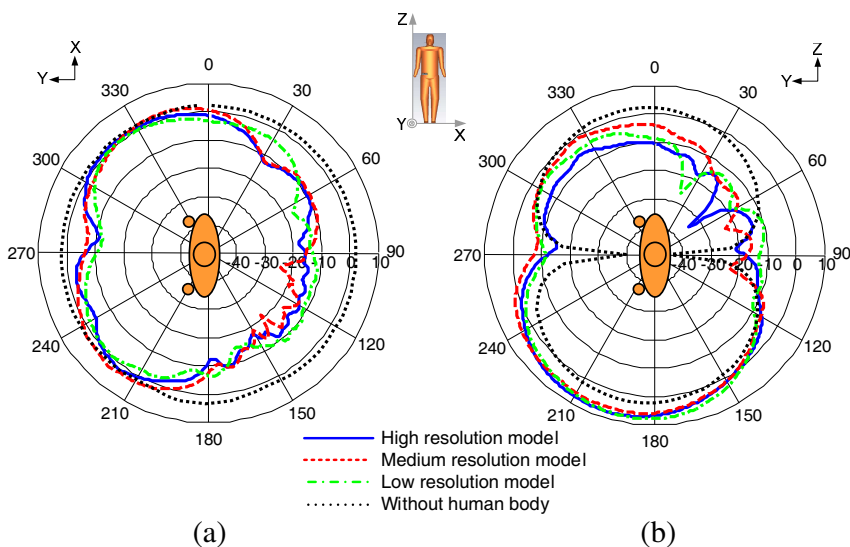


Figure 4. Comparison of simulated 2-D radiation patterns of headset meander line monopole antenna at 2440 MHz using different human body models. (a) XY plane. (b) YZ plane.

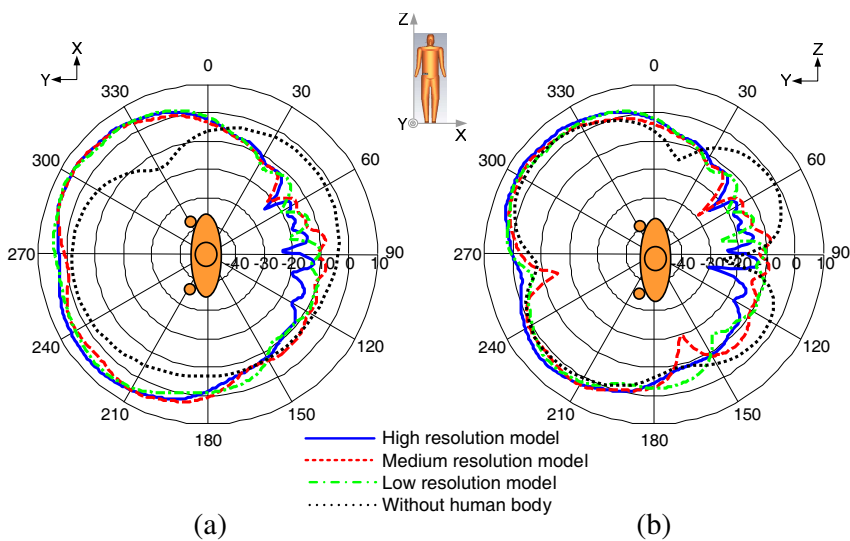


Figure 5. Comparison of simulated 2-D radiation patterns of handset PIFA antenna at 2440 MHz using different human body models. (a) XY plane. (b) YZ plane.

two antennas. Figure 4 highlights the effect of the three models on the radiation pattern of the headset antenna in XY and YZ planes while Figure 5 shows these effects on the radiation pattern of the handset antenna. These results depict that the human body deforms the radiation patterns of the two antennas due to electromagnetic absorptions in the body tissues and reflections from the body surface. It has caused up to 12 dB reduction in the back lobes and 6 dB increase in the frontal radiations for the handset antenna. The effect is more visible on the headset antenna due to the presence of body mass both at side (i.e., head) and underneath (i.e., shoulder) decreasing its radiation in both directions in XY plane. Effect of the head is dominant in YZ plane reducing its radiation between 0–90 degrees. Overall, the radiation patterns of the two antenna are not much influenced by the type of the human body model as results are similar for the three models in terms of deformation trend and gain values.

4.3. Electric Field Distribution

The electric field distributions on the body surface are investigated and compared for the three models. Figure 6 shows distributions of normalised electric field magnitude, viewed on the cross-section

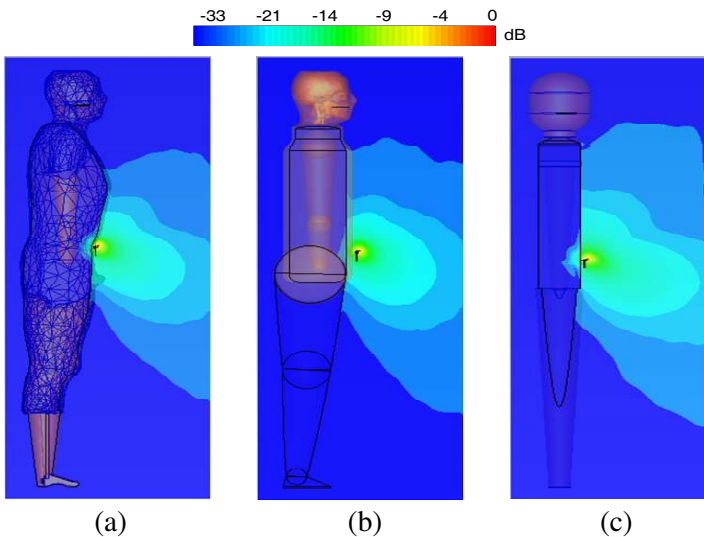


Figure 6. Comparison of normalised electric field distributions on the three human body models for handset antenna on the cross section plane through the headset and handset antennas. (a) High-resolution model. (b) Medium-resolution model. (c) Low-resolution model.

plane (as illustrated in Figure 2(a)) through the headset and handset antennas. The fields are normalised to the value at the feeding point of the handset antenna. From these results, it is obvious that the three models support a similar field pattern. In the three cases, the field strength at the headset antenna is in the order of -18 dB.

The electric field strength for the handset antenna is also plotted as a function of distance between the headset and handset antennas. The field strength is calculated on fourteen curves defined to cover the computational domain between the two antennas. The origin of the three axes for this calculation is located on the right side of the body, above the handset antenna. The starting point in vertical direction (the origin of z -axis) for all the plots is chosen 180 mm away from the

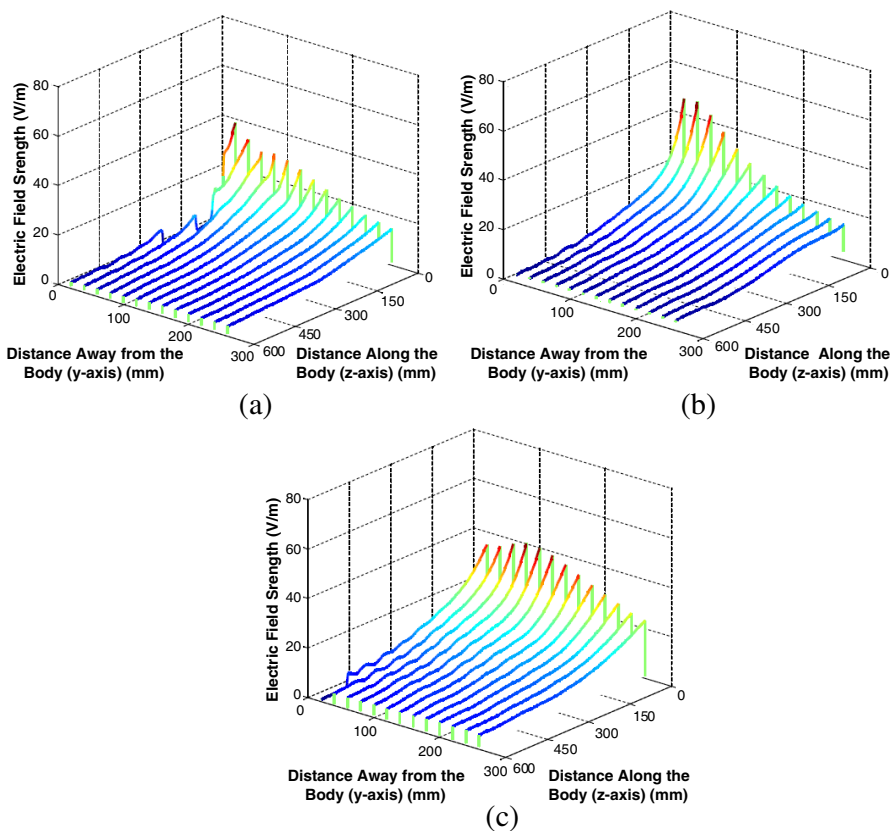


Figure 7. Electric field strength on the curves between the handset and the headset antennas in front of the three body models, corresponding to Figure 2(a). (a) High-resolution model. (b) Medium-resolution model. (c) Low-resolution model.

handset antenna to avoid the antenna near field region as shown in Figure 2(a).

The electric field strength in front of the human body, starting from the body surface and extending to a separation of 280 mm is presented in Figure 7. It is observed that body shape is an important factor that affects the on-body field strength as the field values are very low in the chest region of the high resolution model. On the first curve, the maximum value in this region is observed to be 9 V/m for the high resolution model as compared to 27 V/m for the medium resolution and low resolution models. However, going slightly away from the body makes the results similar for the three models. This, along with the field distributions shown in Figure 6 confirms that the three models generate similar electric field pattern with almost similar strengths for the studied on-body Bluetooth communication link.

4.4. Specific Absorption Rate (SAR)

The Specific Absorption Rate (SAR) is commonly used as a measure to determine the health hazards posed by the RF signal to the human body. It is estimated as whole-body or localised SAR. The localised SAR is determined over 10 g or 1 g volumes of the tissues. The SAR is expressed as follows:

$$\text{SAR} = \frac{\sigma}{\rho} |E|^2 \quad (\text{W/kg}) \quad (1)$$

where, σ is conductivity of the tissue in S/m, ρ is mass density of the tissue in kg/m^3 and E is total RMS electric field strength in V/m.

Different standardisation bodies use certain SAR limits for wireless devices to guarantee the safety of the user. These limits are different for controlled (occupational) and un-controlled (public) conditions of exposure to RF energy. The Federal Communications Commission (FCC) uses 1.6 W/kg SAR value averaged over 1 g of tissue volume as a public safety standard while International Commission on Non-Ionising Radiation Protection (ICNIRP) and The Institute of Electrical and Electronics Engineers (IEEE) have adopted 2 W/kg SAR value averaged over 10 g of tissue volume. The whole body averaged SAR limit is 0.08 W/kg for both the FCC and ICNIRP/IEEE [21, 22]. In this study, European SAR standard of ICNIRP is considered.

The whole-body, 10 g averaged and 1 g averaged SAR for the handset antenna having 1 W (peak) incident power at 2440 MHz have been evaluated and summarised in Table 2. The maximum SAR distributions are compared for the three numerical models in Figure 8. It is evident from this figure that the three models support overall a similar pattern of SAR distribution. For the handset antenna, the SAR

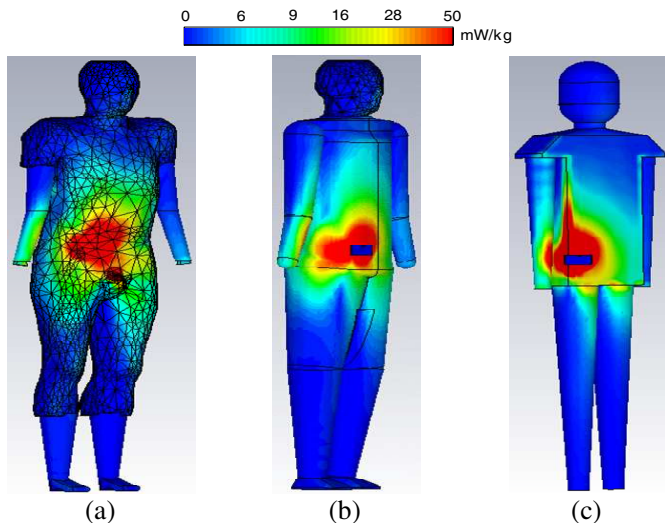


Figure 8. Comparison of maximum SAR distributions on the three human body models for handset antenna. (a) High-resolution model. (b) Medium-resolution model. (c) Low-resolution model.

Table 2. Comparison of 10 g, 1 g and whole-body averaged SAR values at 2440 MHz for handset antenna using high, medium and low resolution numerical models of the human body.

Body model	SAR (W/kg)		
	10 g averaged	1 g averaged	Whole-body
High resolution	1.7	2.7	0.0021
Medium resolution	1.2	2.1	0.001
Low resolution	0.8	1.8	0.0009

is more intense at the pocket position (where the antenna is placed) as this area is directly exposed to the feeding port of the antenna. The location for the maximum SAR value is observed to be similar for the three models.

The level of energy absorption is different in the three models due to varying body shapes. The 10 g averaged SAR values are observed to be 1.7 W/kg, 1.2 W/kg and 0.8 W/kg; the 1 g averaged SAR values are noted to be 2.7 W/kg, 2.1 W/kg and 1.8 W/kg while the whole-body averaged SAR is 0.0021 W/kg, 0.0001 W/kg and 0.0009 W/kg for the high resolution model, medium resolution model and low resolution model, respectively. The trend in change of SAR values with body shape is similar for the three averaging methods and in correspondence to the variation in the electric field strength.

4.5. Comparison of Three Body Models

The observed values of transmission coefficient (S_{21}), electric field strength, maximum SAR and computational efficiency in terms of mesh size and simulation time for the on-body Bluetooth communication link using three human body models are summarised in Table 3.

It is evident from the presented results that numerical modelling of human body is a complex task and needs great care. Different parameters can be affected by the body type, shape and size. Moreover, resolution of the body model affects the computational resources significantly. For the on-body transmission coefficient and electric field strength, the three models give close values with little relative difference. The medium resolution model is giving the closest value to the high resolution model with a maximum relative difference of 5.7% for electric field strength. Low resolution model value differ more with a maximum relative difference of 9.6%. The maximum SAR is affected the most by the type of the model as medium resolution model has a relative difference of 22% while it becomes 33% for the low resolution model. Since the different models have different mass and shape, the absorbed power and SAR have obvious differences. Location of maximum SAR remains close to the feeding port of the

Table 3. Comparison of simulated parameters of on-body Bluetooth communication channel using high-, medium- and low-resolution human body models (with reference to high-resolution model).

Parameter		Performance		
		High	Medium	Low
S_{21}	Value (dB)	-48.3	-47.7	-49.5
	Rel. Difference (%)	—	1.2	2.4
Electric field strength	Value (V/m)	38.4	36.2	42.1
	Rel. Difference (%)	—	5.7	9.6
Maximum SAR	Value (W/kg)	2.7	2.1	1.8
	Rel. Difference (%)	—	22	33
Computational Efficiency	Mesh cells (millions)	186	154	114
	Simulation time (hours)	128	105	75

handset antenna and hence, near to the right side of the bally for the three models.

These results show that for on-body Bluetooth transmission studies, the medium resolution model provides significant accuracy compared with the high resolution model due to good approximation to the real body physique, relatively fast computation and close agreement between the values observed for different parameters to the values offered by the high resolution model and measurement (S_{21}).

5. CONCLUSION

Use of numerical phantoms is a powerful tool for the efficient deployment of BCWNs. It provides easy means to evaluate the electromagnetic interaction of human body and antennas. Selection of a suitable human body model is pivotal in such studies defining the accuracy of the required results, computational time and resources. In this study, three types of the homogeneous human body models; high resolution realistic model, medium resolution flexible simplified model and low resolution basic model are characterised studying different parameters of an on-body Bluetooth communication link between a handset and headset antenna. The results indicate that higher accuracy can be obtained using very realistic models but it requires complex simulation set-up with increased computational requirements. Close agreement between the measured and simulated values of path gain have however indicated that medium resolution simplified human body models can also provide accurate results while improving computational efficiency.

Comparison of the path gain, radiation pattern, electric field strength and SAR distributions shows that for this on-body Bluetooth transmission scenario, the three models behave in an overall similar fashion. The type of the model has less significant impact on the antenna radiation pattern while relative difference between the values of path gain and electric field strength is small. However, for the SAR, this difference is more than 22% between the high resolution and medium resolution models. It is therefore deduced that for on-body Bluetooth transmission studies, relatively low resolution models can be used maintaining significant level of accuracy of the results. However, SAR studies that are necessary for safety guidelines should employ detailed high resolution numerical models of the human body. Further work would be carried out to affirm the usability of this approach in varying body postures and antenna positions on the accuracy of the results.

ACKNOWLEDGMENT

The authors would like to thank Sony Ericsson Communications AB, Sweden and Dstl, UK for their contribution to this study.

REFERENCES

1. Hall, P. S. and Y. Hao (eds.), *Antennas and Propagation for Body-Centric Wireless Networks*, 2nd edition, Artech House Inc., London, 2012.
2. Chen, Z. N., *Antennas for Portable Devices*, John Wiley and Sons, Inc., UK, 2007.
3. Toftgard, J., S. Hornsleth, and J. B. Anderson, "Effects on portable antennas of the presence of a person," *IEEE Transactions on Antennas and Propagation*, Vol. 41, No. 6, 739–746, 1993.
4. Jensen, M. A. and Y. Rahmat-Samii, "EM interaction of handset antennas and human in personal communications," *IEEE Proceedings on Antennas and Propagation*, Vol. 83, No. 1, 7–17, 1995.
5. Okoniewski, M. and M. A. Stuchly, "A study of the handset antenna and human body interaction," *IEEE Transactions on Microwave Theory and Techniques*, Vol. 44, No. 10, 1855–1864, 1996.
6. Wang, Z., X. Chen, and C. G. Parini, "Effects of the ground and the human body on the performance of a handset antenna," *IEE Proceedings on Microwave, Antenna and Propagation*, Vol. 151, No. 2, 131–134, 2004.
7. Chen, Z. N., A. Cai, T. S. P. See, X. Qing, and M. Y. W. Chia, "Small planar UWB antennas in proximity of the human head," *IEEE Transactions on Microwave Theory and Techniques*, Vol. 54, No. 4, 1846–1857, 2006.
8. Conway, G. A., W. G. Scanlon, and D. Linton, "Low-profile microstrip patch antenna for over-body surface communication at 2.45GHz," *IEEE Vehicular Technology Conference*, April 2007.
9. Drude, S., "Requirements and application scenarios for body area networks," *Mobile and Wireless Communications Summit*, 1–5, 2007.
10. Nagaoka, T., S. Watanabe, K. Sakurai, E. Kunieda, M. Taki, and Y. Yamanaka, "Development of realistic high-resolution whole-body voxel models of Japanese adult males and females of average height and weight, and application of models to radio-frequency electromagnetic-field dosimetry," *Physics in Medicine and Biology*, Vol. 49, No. 4, 1–15, 2003.

11. Tell, R. A., "Microwave energy absorption in tissue," *Twinbrook Research Laboratory Technical Report*, 1972.
12. Weil, C. M., "Absorption characteristics of multilayered sphere models exposed to UHF/microwave radiation," *IEEE Transactions on Biomedical Engineering*, Vol. 22, No. 6, 468–476, 1975.
13. COST244 Working Group 3, "Proposal numerical canonical models in mobile communications," *Proceedings of COST 244*, 1–7, Rome, Italy, November 1994.
14. Nishizawa, S. and O. Hashimoto, "Effective shielding analysis for three layered human model," *IEEE Transactions on Microwave Theory and Techniques*, Vol. 47, No. 3, 277–283, 1999.
15. Hao, Y., "Numerical and system modelling issues in body-centric wireless communications," *The IET Seminar on Antennas and Propagation for Body-Centric Wireless Communications*, April 2007.
16. Hombach, V., K. Meier, M. Burkhardt, E. Kuhn, and N. Kuster, "The dependence of EM energy absorption upon human head modelling at 900 MHz," *IEEE Transactions on Microwave Theory and Techniques*, Vol. 44, No. 10, 1865–1873, 1996.
17. Holden, S. J., R. D. Sheridan, T. J. Coffey, R. A. Scaramuzza, and P. Diamantopoulos, "Electromagnetic modelling of current flow in the heart from TASER devices and the risk of cardiac dysrhythmias," *Physics in Medicine and Biology*, Vol. 52, 7193–7209, 2007.
18. Ur Rehman, M., Y. Gao, Z. Wang, J. Zhang, Y. Alfadhl, X. Chen, C. G. Parini, Z. Ying, T. Bolin, and J. W. Zweers, "Investigation of on-body bluetooth transmission," *IET Proceedings Microwaves, Antennas and Propagation*, Vol. 4, No. 7, 871–880, 2010.
19. Gabriel, C., "Compilation of the dielectric properties of body tissues at RF and microwave frequencies," *Brooks Air Force Technical Report*, AL/OE-TR-1996-0037, 1996 (FCC website, <http://www.fcc.gov/oet/rfsafety/dielectric.html>).
20. CST Microwave Studio[®] 2013 User Manual.
21. FCC OET Bulletin 65, "Evaluating compliance with FCC guidelines for human exposure to radiofrequency electromagnetic fields," FCC, August 1997.
22. "ICNIRP guidelines for limiting exposure to time-varying electric, magnetic and electromagnetic fields (up to 300 GHz)," (ICNIRP website, <http://www.icnirp.de/documents/emfgdl.pdf>).